Landslide Hazard Zonation and Evaluation Around Debre Markos Town, NW Ethiopia—A GIS-Based Statistical Approach

Dawit Asmare Manderso (dawitasmare55@gmail.com)
Debre Markos University College of Technology https://orcid.org/0000-0002-6731-195X

Research Article

Keywords: Landslide hazard evaluation, Hazard index, Landslide hazard zonation, landslide inventory

Posted Date: June 2nd, 2021

DOI: https://doi.org/10.21203/rs.3.rs-541709/v1

Abstract

The main goal of this research was to perform a landslide hazard zonation and evaluation around Debre Markos town, North West Ethiopia, found about 300 km from the capital city Addis Ababa. To achieve the aim, a GIS-based probabilistic statistical technique was used to rate the governing factors, followed by geoprocessing in the GIS setting to produce the landslide hazard zonation map. In this research, eight internal causative and external triggering factors were selected: slope material (lithology and soil mass), elevation, aspect, slope, land use land cover, curvature, distance to fault, and distance to drainage. Data were collected from field mapping, secondary maps, and digital elevation models. Systematic and detailed fieldwork had been done for image interpretation and inventory mapping. Accordingly, the past landslides map of the research area was prepared. All influencing factors were statistically analyzed to determine their relationship to previous landslides.

The results revealed that 17.15% (40.60 km2), 25.53% (60.45 km2), 28.04% (66.39 km2), 18.93% (44.83 km2), and 10.36% (24.54 km2) of the research area falls under no hazard, low hazard, moderate hazard, high hazard, and very high hazard respectively. The validation of the landslide hazard zonation map reveals that 1%, 2%, 3%, and 94% of past landslides fall in no hazard zone, low hazard, moderate hazard zone, and high hazard or very high hazard zones respectively. The validation of the landslide hazard zonation map thus, it has been adequately demonstrated that the adopted approach has produced acceptable results. The defined hazard zones can practically be utilized for land management and infrastructure construction in the study area.

Introduction

Landslides are the most frequent and severe geologic hazards in hilly areas, causing immediate economic harm, property damage and repair costs, injuries, and death *(Kumar and Anbalagan, 2015; Dai and Lee, 2011; Ali et al., 2015; Pantelidis, 2009; Wang et al., 2015; Ermias et al., 2017;* Asmare and Hailemariam, 2021*; Woldearegay, 2013; Chen et al., 2017; Wang et al., 2015; Saha et al., 2010; Hamza and Raghuvanshi, 2016).*

The Ethiopian highlands are defined by geomorphological conditions, complex geological conditions, poor soil cover, heavy rains, and hydrological and hydro geological factors *(Chimidi et al., 2017;Ayalew and Yamagishi, 2004; Ayalew and Yamagishi 2005; Hamza and Raghuvanshi 2017; Woldearegay, 2013; Raghuvanshi et al., 2014)*. These conditions are usually responsible for massive to small landslides. According to the Ayalew and Yamagishi (2005) description in Ethiopia, slope failures occur in wide regions with distinctive slope materials, geological structures, and topographical settings.

Several geo-environmental processes including geological, metrological, and human activities are highly responsible for the landslides *(Kumar and Anbalagan, 2015)*. According to *Raghuvanshi et al. (2014)* presentation, the slope geometry, slope material, structural discontinuities, land use land cover, slope

geometry, and groun dwater are the main intrinsic parameters, while excessive rainfall, earthquakes, and man-made activities can be considered as the main causative factors for landslides.

Landslide hazard zoning (LHZ) was carried out according to various approaches. Such approaches can be categorized into three main classes; deterministic method, statistical approaches, and expert evaluation method *(Karaman et al., 2006b; Fall et a., 2006; Dai and Lee, 2001; Du et al., 2017; Westen, 1993; Westen et al., 2003).* Selection of approaches for landslide hazard zoning depends on the size of the analysis to be performed, the total coverage area, expertise, and skill set of evaluators, the geological or geomorphic parameters or methods used to produce parameter data *(Fall et al., 2006*; *Carrara et al., 1992; Ermias et al., 2017).*

The main aim of this research was to produce a landslide hazard zonation (LHZ) map for the area. Thus, a GIS-based landslide hazard evaluation and zonation method was used to produce the LHZ map.

Study area

The current research area is situated in the east-central region of the North-Western Ethiopian Plateau (NWP), in the East Gojjam district of the Amhara Regional State. The area covers small parts of Gozamin, Aneded, and Baso Liben districts as shown in Fig.1. It covers an area of nearly 236.8 km^2. The study area can be accessed via Addis Ababa to Debre Werek main Asphalt road which is about 300 Km and then 27 km gravel road towards Yejube town. The area is generally not easily accessible by vehicles, and there are no standard routes to reach throughout all parts of the research area. The type of soil and its landscape is difficult to go through various regions of the research area.

Regional geology

The research area is situated in the Northwestern Plateau, which is distinguished by the geology of the Abay basin. The basin comprises of Precambrian basement, Paleozoic and Mesozoic sedimentary rocks, Tertiary to Quaternary volcanic rocks, and Quaternary deposits *(Russo et al.,1994; Assefa, 1991; Lebenie and Bussert, 2009; Lebenie, 2010; Gani et al, 2008; Gani and Abdelsalam, 2006; Mogessie et al., 2002; Ahmed, 2008, 2009, 2010; Ismail and Abdelsalam, 2012; Braathen et al. 2001).* According to the regional map prepared by Tefera et al. (1996), the present area comprises different geological formations including Tarmaber Gussa, Ashange formation, Adigrat formation. The Tarmaber Gussa formation is distinguished by alkaline to transitional basalts that often form shield volcanoes and contain minor trachyte and phonolite flows, as well as Late Proterozoic Ultramafic rock composed of serpentinite, peridotite, dunite, and talc schists. The Ashangi formation is distinguished by strongly weathered alkaline and transitional basalt flows with unusual tuff intercalation, which is often tilted (contains Akobo basalts of SW Ethiopia). Adigrat formation is characterized by Triassic- Middle Jurassic sandstone.

Local geology

Field surveys and secondary data sources were used to map the geology of the present research area. It consists of basalt, sandstone, alluvial deposits, colluvial deposits, and residual soils. The lithologies are visible throughout road cuts and on natural hillsides. The basalt unit is affected by a slightly to complete degree of weathering.

Methodology

This research was divided into three major phases: data collection, data processing and manipulation, analysis, and the development of an LHZ chart. The data collection phase of the study focuses on collecting existing topographical and geological maps, as well as conducting fieldwork to visually examine the lithologic units and develop a landslide inventory map.

The probabilistic statistical approach was used for landslide hazard zonation. This approach can provide practical interactions between different triggers and landslide distribution in the past and present. It consists of a landslide inventory mapping accompanied by the production of a predictive hazard model based on eight triggering factors and their relationships with previous landslides *(Hamza & Raghuvanshi, 2017).* The causative factors are; slope material (soil and rock), slope, aspect, elevation, ground water surface traces, curvature, distance to streams, and distance to roads. Finally, the landslide zonation map was produced based on the relative influence of various causative factors.

The statistical approach is used within each causative factor map and its parameter map classes to determine the densities of landslides *(Wahono, 2010;Hamza & Raghuvanshi, 2016).* Later, depending on the class distribution and landslide density, corresponding weights can be developed *(Hamza & Raghuvanshi, 2017)*. The quantitative prediction was made using the density ratio of past landslides with the various factor classes. This helps to rate the various causatives that are responsible for the reoccurrence of landslides with similar conditions in the area *(Shahabi et al., 2013; Hamza & Raghuvanshi, 2016)*. As a result, factor maps were integrated with the derived weights to obtain a landslide hazard zonation map.

The system followed in this research is based on the expectation that the causatives responsible were considered. The number of grid cells and a hazard index value can be used to determine these causative factors. This can lead directly to a landslide hazard assessment. The ratio of landslides that 'did' occur to landslides that 'did not occur' is the hazard index value of all factors *(Chimidi et al., 2017)*. Later, based on the values of hazard indexes, equivalent weight was assigned for all factors. Then, using all six responsible factor layers, generic trial combinations were developed. Thus, landslide hazard evaluation was computed using the optimal combination of internal causative and external triggering factors. The actual data obtained from previous landslides was used to verify the developed landslide hazard zonation map of the research area.

5. Data collection and analysis

In this research, primary and secondary data were used. Secondary data sources include DEM, satellite images, topographical maps, and meteorological data. The primary goal of the field investigation was to collect relevant information on the previous landslide and to validate the different factor maps developed.

The controlling factors including slope angle, slope aspect, and elevation were computed using a DEM obtained from the ASTER satellite. Lithological information was obtained from the geological map of Ethiopia (scale 1: 2.000,000), while Landsat + ETM data can be used to process land use land cover and soil cover.

5.1. Landslide inventory mapping

A landslide inventory map is important to landslide hazard mapping. It is frequently accepted that the conditions that caused previous landslides can cause landslides again if they occur elsewhere in the given area *(Raghuvanshi et al.,2015; Lan et al., 2004; Dai et al., 2002).*

In the present research, past landslide and no past landslide areas are delineated through extensive field works. Accordingly, the Landslide inventory map was created by overlaying field GPS failure point data on the areal photo and DEM_30m obtained from the USGS data source by using Arc GIS 10.5 (Fig.2). All maps in this study were produced at a scale of 1:50,000. During field work, most past landslides were observed following fault structures (Fig.2). Besides, there are also a significant number of landslide activities following rives and valleys.

5.2. Evaluation of causative factors

The frequency of landslides is affected by the interaction of several factors, including topographic, hydrological, and geological factors; therefore, selecting the causative factors is regarded as a critical issue in LHZ mapping (Dou et al., 2015)

In this research, based on field observation and contribution to previous landslides, eight influential causative factors were selected. These include lithology and soil mass, slope, aspect, elevation, curvature, land use land cover, and distance from the stream, and distance from lineaments/fault. These factors were identified based on field observations of previous landslides and their contribution to slope instability.

5.2.1. Lithology and soil mass

The lithology has a significant effect on slope stability; various lithological units have varying degrees of susceptibility (Anis et al., 2019). Lithology has a significant impact on the stability of the soil, natural ground cover, and features created by human activities (Varo et al.,2019). Landslides are more likely in areas where the rocks are weak, poorly consolidated, and incompetent (Kailas et al., 2018).

The lithological map of the research area was updated from the Geological Map produced by Tefera et al. (1996) and through extensive field investigations (Fig. 3A). Past landslide distribution shows that 10.5%

of the landslides occurred in Adigrat formation,1.8% of the landslides occurred in Ashangi formation, 1.6% of the landslides occurred in Tarmaber formation, 23.7% of the landslides occurred in alluvial soil, 51.5% of the landslides occurred in colluvial soil, 10.9% of the landslides occurred in residual soil.

5.2.2. Slope

Slope angle is among the most important factors influencing landslides (Kailas et al., 2018; Varo et al., 2019) because it is directly linked to landslides (Yalcin, 2008). In general, the steeper slope the chances of landslide occurrence are increases (Kailas et al., 2018). Gravity pulls are directly related to the slope angle, which is the primary driving force for slope failure (Bisson et al., 2013, 2014, 2010; Raghuvanshi et al., 2014). DEM was used to produce a slope map of the research area. Accordingly, the slope angle classes are; very gentle slope (<15°), gentle slope (16–25°), moderately steep slope (26–35°), steep slope (36–45°), and escarpment /cliff (>45°) as shown in Fig. 3B.

According to the landslides inventory data, the spatial and potential distribution of landslides revealed that 1.6% o, 11.3%, 22.4%, 21%, 16.7% and 27% of the landslides occurred in the slope classes between 0–5°,5–14°,14–25°,25–35°,35–45° and 45° respectively.

5.2.3. Elevation

Higher elevation areas have a higher possibility of landslide occurrence than lower elevation areas (Kailas et al., 2018). Lower elevation terrain is usually gentle, and a high water table is needed to trigger slope failure (Kailas et al., 2018).

For this study, elevation was sub-classified into five classes from 1283–1544m, 1544–1764m, 1764–1994m, 1994–2221m, and 2221–2500m (Fig. 3C). The distribution of landslides from past landslide inventory data revealed that 18.7%, 21.1% 17.8%, 23%, and 18.6% of the landslides occurred in the slope classes from 1283–1544m, 1544–1764m, 1764–1994m, 1994–2221m, and 2221–2500m respectively.

5.2.4. Aspect

The direction of the slope in respect to the sunlight has a huge effect on its structural and chemical composition of the soil slope (Das et al.,2014; Anis et al., 2019; Abay et al., 2019). The DEM was used to compute the slope aspect map of the research area. In this study, aspect was classified into nine classes; Flat (-1°), North (0–22.5°), Northeast (22.5–67.5°), East (67.5–112.5°), Southeast (112.5–157.5°), South (157.5–202.5°), Southwest (202.5–247.5°), West (247.5–292.5°), Northwest (292.5–337.5°) and North (337.5-360) (Fig. 3D).

Accordingly, 0.02% of landsides occurred in Flat surfaces, 6.5% of landsides occurred in slopes facing North, 6.1% of landsides occurred in slopes facing Northeast,3% of landsides occurred in slopes facing East, 3.6 % Southeast, 6.5% of landsides occurred in slopes facing South,13.7% of landsides occurred in slopes facing Southwest, 24.1% of landsides occurred in slopes facing West, 27.1% of landsides occurred in slopes facing Northwest and the remaining 9.4% of landsides occurred in slopes facing North direction.

The distribution of previous landslides in the area concerning aspect shows that the majority of landslides concentrated on slopes inclined toward the West and Northwest directions.

5.2.5. Land Use Land Cover

The strength of slope materials against sliding and the regulation of slope water content are affected by land use land cover (Bchari et al., 2019). Furthermore, plant roots strengthen the slope and are commonly regarded as reinforcements (Bchari et al., 2019). Land cover absorbs soil water and decreases the probability of a landslide (Bchari et al., 2019).

Secondary data and the Landsat image collected from the USGS data source were used to develop a land use land cover map. Then, the map was modified and updated based on visual field observation, and the final map was produced (Fig. 3E) in Arc GIS. Later, to assign SSEP ratings for the individual facet, facet wise percentage area coverage of land use - the land cover was generated by geoprocessing in the GIS environment.

The occurrence of landslides within different land use land cover categories reveals (Fig. 3E) that 1.4% of landslides occurred within the forest, 0.8% of landslides occurred within grazing land, 22.6% of landslides occurred within bush land, 24.2% of landslides occurred within barren land and the remaining 51% were recorded within cultivated land.

5.2.6 Curvature

The morphology of the topography is represented by the curvature values (Nohani et al., 2019; Foumelis et al., 2018;). This factor affects landslide occurrence while controlling surface runoff (Nohani et al., 2019).

DEM was used to develop a curvature map of the research area and this was divided into three main classes: concave (0), zero curvature (flat (0)), and positive curvature (convex (>0)) (Fig. 3F). The slope's concavity is shown by a negative curvature value, while the slope's convexity is showed by a positive curvature value. High convexity and concavity cause drainage concentration across space, resulting in slope saturation and instability (Mandal & Mandal, 2018). Accordingly, in the present study, 49.2% of landsides occurred in concave slope (<0), 1.1% of landsides occurred in flat slope (0) and 49.6% of landsides occurred in convex slope (>0).

5.2.7 Distance to drainage

The saturation degree of the slope's material is a significant parameter that governs its stability (Anis et al., 2019; Yalcin, 2008). This other important factor in slope stability is the slope's proximity to drainage systems (Yalcin, 2008). River water is considered the main source of soil moisture (Nohani et al., 2019). Proximity to drainage lines of intensive gully erosion is a crucial factor controlling the occurrence of landslides (Foumelis et al., 2018)

Similar to other causative factors, DEM was used to create a drainage network, and this was computed in ArcGIS using Euclidean distance. Then, the distance to drainage was classified into five classes; 0–298m, 298–604m, 604–902m, 902–1249m, and 1249–2055m (Fig. 3G).

The distribution of landslides from previous landslide inventory data revealed that 44.9%, 25.5%,15.5%, 9.5%, and 4.5% of the landslides occurred in the drainage distance class 0–298m, 298–604m, 604–-902m, 902–1249m, and 1249–2055m respectively.

5.2.8 Distance to fault

Geological structures including folds, joints, bedding, and shear zones faults have a greater impact on slope stability (Michael & Samanta, 2016). The proximity of a slope to these features has a significant impact on its stability, increasing the probability of landslides occurring (Michael & Samanta, 2016). The number of joints in a rock reduces its strength, which increases the distance to faults/lineaments.

The fault map was created using a Google Earth image, a geological map, and DEM 30m data from the USGS. The distance to fault was generated by Euclidean distance in ArcGIS, then reclassified into six classes; 0–500m, 500–2000m, 2000–2500m, 2500–5000m, 5000–6500m, and > 6500m (Fig. 3H). The distribution of landslides from past landslide inventory data revealed that 77.9%, 20%, 0.9%, 0.1%, 1%, and 0.1% of the landslides occurred in the fault distance class between 0–500m, 500–2000m, 2000–2500m, 2500–-5000m, 5000–6500m and greater than 6500m respectively.

5.3. Landslide hazard evaluation

In this research, a bivariate statistical system was applied to develop an LHZ map. The densities of each factor were used to assign every factor. These were statistically integrated to produce the LHZ map of the research area (Mandal & Mandal, 2018; Chimidi et al., 2017; Suzen and Doyuran, 2004; Hamza & Raghuvanshi, 2017; Chimidi et al., 2017). The bivariate analyses are important to quantify the abundances of the landslide within each percentile class (Süzen & Doyuran, 2004). In each causative factor class, hazard index value' was used, obtained from the ratio of landslides that 'did' occur to landslides that 'didn't occur within each factor class. Thus, hazard index values were used to determine hazard classes and the weight assigned to each factor.

The quantitative relationships were determined by processing landslide inventory maps and all factor maps in a GIS environment. Thus, The total pixel count was calculated for each factor class where the landslide occurred and did not occur as presented in Tables 2 and 3. Using ArcGIS's raster calculator, the total pixel count for the whole research area was 263,112, while the 80, 276-pixel count was covered by a landslide.

Data preparation

Landslide locations were investigated using extensive field surveying and satellite image interpretation. The whole existing landslide was demarcated using GPS along the fringe, and then polygons were

generated using Google Earth images. Finally, using polygons, a landslide boundaries map was developed. Later, this map was used for landslide data analysis in a GIS environment. Moreover, vector to raster conversion was performed to generate a 30 x 30 m pixel raster data set of past landslides. In addition, an Arc map was used to create a spatial database on the internal causative and external triggering factors such as slop material (lithology and soil mass), elevation, slope, aspect, curvature, land use land cover, distance from the fault/lineament, and distance from drainage. Various data layers that were used to develop landslide hazard zonation maps and for statistical analysis were presented in Table 1.

5.3.3. Landslide Hazard Zonation(LHZ)

In this research, slope material (lithology and soil mass), slope, aspect, elevation, curvature, land use land cover, distance from drainage, and distance from the fault were selected as causative factors. It was believed that these causal factors were most likely to account for the landslides in the area.

The hazard map for each of the eight causal factors was prepared using a weight equal to '1.' (Table 3). The possible explanation for assigning equal weight to all different internal causative and external triggering factors was that the relative contribution of each parameter to slope failure can not be quantified. Therefore, it was assumed that each of these factors would have a relative contribution to slope failure. Using the “raster calculator" tool and ratings, a landslide hazard zonation map of the area was produced.

Results And Discussion

The produced landslide hazard map(Fig. 4), showed that 17.15% (40.60 km2), 25.53% (60.45 km2), 28.04% (66.39 km2), 18.93% (44.83 km2) 10.36% (24.54 km2) area fall in the no hazard, low, moderate, high and very high hazard classes respectively. Consequently, a glance at Fig. 4 reveals that very high hazard (VHH) areas generally fall in southwestern parts of the areas, while southern and southwestern parts are demarcated as high hazard (HH) zones, with a scarce distribution in the eastern and northern part. In addition, moderate hazard (MH) zones are widely distributed in the eastern and northern regions, while Low hazard (LH) are distributed in the northwestern region of the research area. More dispersed Low hazards areas are also found in the central and eastern regions. No-hazard (NH) areas are mostly clustered in the north, with a sparse distribution in the west and east.

The prevalence of colluvial and alluvial soils, relatively gentle slopes (14–25), and elevation class 1821–1954m are all factors that contribute to the wide distribution of the Very high hazard(VHH) zone and high hazard (HH) zone in the southwestern area. Most likely landslides occur on slopes with an angle of 14–25, according to previous landslide inventory data, with 82 % of landslides occurring only on this slope class. The majority of prone slopes are covered with alluvial and colluvium soil. furthermore, nearly 68% of past landslides were distributed following the elevation class 1821–1954m. This indicates that this elevation class is the most vulnerable to slope failure.

6.1. LHZ map validation

The landslide hazard map was validated with the help of past landslide locations. This was computed by overlaying landslide location data and landslide hazard map produced in this research. According to the overlay analysis (Fig. 5), 70% of past landslides were found in the very high hazard zone and 24% are in the high hazard zone. Therefore, 94 % of past landslide locations were satisfactorily matched with the LHZ map. The remaining 3% of landslides are found in the moderate hazard zones, 2% are found in the low hazard zones, and 1% are found in the no hazard zones. Furthermore, the produced landslide hazard map was physically validated in the field at several regions, most notably in the very high hazard and high hazard zones. Landslide activities were observed in areas that defied very high hazard and high hazard zones.

Thus, it is reasonable to assume this landslide hazard map (LHZ) map adequately demarcated the spatial and potential landslide hazard zones of the research area.

Conclusion

The southwestern region of Debre Markos town including Gozamin, Aneded, and Baso Liben districts affected by several landslides every year resulting in damages to infrastructures and propertiesEight governing factors were prepared for this study: lithology and soil mass, slope, elevation, aspect, curvature, land use land cover, distance from lineaments/fault, and distance from drainage. An inventory map of landslides was created using a digital elevation model (DEM), satellite images, and extent field investigation. Using the inventory map, the statistical relationship between governing factors and landslides was investigated, as well as their probable contribution to landslides in the area. In this research, the governing factors were rated using a GIS-based statistical and probability method, and the landslide hazard map was generated using a customized raster calculation. In this study, landslide hazard evaluation showed that 17.15% (40.60 km2), 25.53% (60.45 km2), 28.04% (66.39 km2), 18.93% (44.83 km2) 10.36% (24.54 km2) area fall in the no hazard, low, moderate, high and very high hazard classes respectively.

References

Ahmadi, M., And Eslami, M. (2011). A new approach to plane failure of rock slope stability based on the water flow velocity in discontinuities for the Latian dam reservoir landslide. J. Mt. Sci. 8:124–130.

Ahmed, M. F., Kang, X. And Khan, M. S. (2016). Impact of rainwater infiltration on the stability of Earth slopes. Int. J. Econ. Environ. Geol. 7(2):20–25.

Alexander, D. E. (1999). Landslide; natural disasters. pp 242-266. Kluwer academic publishers, The Netherlands.

Ali, D., Majeed, Y., Shahzad, M., Iqbal, M. M., Liaqat, S., Gill, M. A., and Ali, M. A. (2015). Detailed slope stability analysis of selected slope sites situated along Katas-Choa Saiden shah road. international journal of engineering inventions, 5(1), 32–43.

Anbalagan, R. (1992). Landslide hazard evaluation and zonation mapping in mountainous terrain. Eng. Geol. 32: 269-277.

Asmare, Dawit. and, Hailemariam, Trufat. (2021). Assessment of rock slope stability using slope stability probability classification (SSPC) system, around AlemKetema, Scientific African, 12, e00730. https://doi.org/10.1016/j.sciaf.2021.e00730

Asmelash A. and Barbieri G. (2012). Landslide susceptibility and causative factors evaluation of the landslide area of Debresina, in the southwestern afar escarpment, Ethiopia. journal of earth science and engineering 2: 133-144.

Braathen, A., Grenne, T., Selassie, M.G., and Worku, T. (2001). The juxtaposition of Neoproterozoic units along the Barbuda-Tulu Dimtu shear belt in the East African

Orogen of western Ethiopia. Precamb. Res. 107: 215–234.

Birhanu Ermias, Raghuvanshi, T. K., and Bekele Abebe. (2017). Landslide hazard zonation (LHZ) around Alemketema town, North Showa Zone, Central Ethiopia - a GIS-based expert evaluation approach. international journal of earth sciences and engineering, 10(1), 33–44.

Bommer, J.J., Rodrı´guez, C.E. (2002). Earthquake-induced landslides in Central America.

Eng. Geol. 63, 189–220.

Carrara, A. Cardinali, M., Guzzetti, F. (1992). Uncertainty in assessing landslide hazard and risk, ITC J. 2, PP. 172–183.

Chen, H., Lee, C. F. And Law, K. T. (2004). Causative mechanisms of rainfall-induced fill slope failures. J. Geotech. Geoenviron. Eng. 130:593–602.

Chen, X., Guo, H., And Song, E. (2008). Analysis method for slope stability under rainfall action. Landslides and Eng. Slopes 1507–1515.

Collison, A., Wade, S., Griffiths, J., and Dehn, M. (2000). Modeling the impact of predicted climate change on landslide frequency and magnitude in SE England. Eng. Geol. 55:205-218.

Dahal, R.K., Hasegawa, S., Masuda, T., Yamanaka, M. (2006). Roadside slope failures in

Nepal during torrential rainfall and their mitigation. disaster mitigation of debris

flows, slope failures and landslides, pp. 503–514

Dai, F. C., and Lee, C. F. (2011). Terrain-based mapping of landslide susceptibility using a geographical information system: a case study. Canadian Geot. Journal, 38(5), 911–923.

Dawit Lebenie and Bussert, R. (2009). Stratigraphy and facies architecture of Adigrat sandstone, Blue Nile Basin, Central Ethiopia. Zentral Blatt Geol. Paläont 1(3/4): 217–232.

Dawit Lebenie (2010). Adigrat sandstone in northern and central Ethiopia: Adigrat sandstone in northern and central Ethiopia: stratigraphy, facies, depositional environments, and palynology. Unpublished Ph.D. Thesis, Technische Universität Berlin, German,166 pp.

Du, G., Zhang, Y., Iqbal, J., Yang, Z. and, and Yao, X. (2017). Landslide susceptibility mapping

using an integrated model of information value method and logistic regression in the

Bailongjiang watershed, Gansu Province, China. Journal of Mountain Sci.,14(2), 249–268.

Fall, M. Azzam, R. Noubactep, C. (2006). A multi-method approach to study the stability of natural slopes and landslide susceptibility mapping. Eng. Geol. 82, PP. 241–263.

Gani, N. D., and Abdelsalam, M. G. (2006). Remote sensing analysis of the gorge of the Nile, Ethiopia with emphasis on Dejen – Gohatsion region. J. Afr. Earth Sci. 44:135–150.

Gani, N. D., M. G. Abdelsalam, S. G., and M. R. Gani. (2008). Stratigraphic and structural evolution of the Blue Nile Basin, Northwestern Ethiopian Plateau. Geo. J. 44:30–56.

Getaneh Assefa (1991). Lithostratigraphy and environment of deposition of the late Jurassic - early Cretaceous sequence of the central part of Northwestern Plateau, Ethiopia. N.Jb. Geol. Palaont. Abh. 182(3): 255–284.

Hack, R. (1998). Slope stability probability classification, SSPC. 2nd edn. Vol.43, ITC Delt Pub., Enschede, The Netherlands, 273 pp.

Hack, R. (2002). An evaluation of slope stability classification. In: ISRM EUROCK'2002, Portugal Madeira Funchal, pp. 3 – 32. Lisboa, Portugal.

Hagos Gebreslassie. (2014). Land use-land cover dynamics of Huluka watershed, Central Rift Valley, Ethiopia. Int. Soil and Water Con. Research 2(4):25–33.

Hamza, T., and Raghuvanshi, T. K. (2017). GIS based landslide hazard evaluation and zonation –a case from Jeldu District, Central Ethiopia. Journal of King Saud Univ. Sci., 29, 151-165.

Hays, W.W. (1980). Procedures for estimating earthquake ground motion. U.S. Geol. Surv. Prof. Paper. 1114, 77pp.

Hoek, E., and Bray, J.W. (1981). Rock slope engineering (revised third ed.). Ins. Of Mining and Metallurgy, London, 358Pp.

Ismail, E. H., and Abdelsalam, M. G. (2012). Morpho-tectonic analysis of the Tekeze River and the Blue Nile drainage systems on the Northwestern Plateau, Ethiopia. J. Afr. Earth Sci. 69:34–47.

Jaboyedoff, M., Baillifard, F., Bardou, E., and Girod, F. (2004). The effect of weathering on Alpine rock instability. Quarterly J. Eng. Geo. And Hydrogeo. 37:95–103.

Johnson, R.B., Degraff, J.V. (1991). Principles of Engineering Geology. John Willy and Sons, New York, pp. 497.

Kanungo, D. P., Arora, M. K., Sarkar, S., and Gupta, R. P. (2006a). Landslide susceptibility

zonation (LHZ) Mapping – A Review. Journal of South Asia Disaster Studies 2. PP1-81.

Kanungo, D.P., Arora, M.K., Sarkar, S., Gupta, R.P. (2006b). “A comparative study of conventional, ANN black box, fuzzy and combined neural and fuzzy weighting procedures for landslide susceptibility zonation in Darjeeling Himalayas”. Eng. Geol. 85, PP. 347–366.

Karaman, K., Ercikdi, B., And Kesimal, A. (2013). The assessment of slope stability and rock excavatability in a limestone quarry. Earth Sci. Res. Sj. 17(2):169–181.

Keefer, D.V. (2000). “Statistical analysis of an earthquake-induced landslide distribution – the 1989 Loma Prieta, California event”. Eng. Geol. 58, PP. 231–249.

Kifle Woldearegay. (2013). Review of the occurrences and influencing factors of landslides in the highlands of Ethiopia: with implications for infrastructural development. Momona Ethiopian Journal of Science (Mejs), 5(1996), 3–31.

Laike Mariam Asfaw (1986). Environmental hazard from fissures in the Main Ethiopian Rift. J. Affr. Earth. Sci. 27 (3/4): 481 - 490.

Lee S, Min K. (2001) Statistical analysis of landslide susceptibility at Yongin. Korean Environ Geol 40:1095–1113.

Li, X. Z. and Xu, Q. (2015). Application of the sspc method in the stability assessment of highway rock slopes in the Yunnan province of China. Bull.Eng.Geol.Env. 75(2): 551-562.

Lulseged Ayalew and Yamagishi, H. (2005). The application of GIS-based logistic regression for landslide susceptibility mapping in the Kakuda-Yahiko Mountains, Central Japan, 65, 15–31.

Lulseged Ayalew and Yamagishi, H. (2004). slope failures in the Blue Nile basin, as seen from a landscape evolution perspective, 57, 95–116.

Lulseged Ayalew, Yamagishi, H., and Ugawa, N. (2004). Landslide susceptibility mapping using GIS-based weighted linear combination, the case in Tsugawa area of Agano River, Niigata Prefecture, Japan. Landslides. 1:73–81.

Mangesha, Tefera, Tewedros Chernet, and Workneh Haro (1996). Geological map of Ethiopia (1:2,000,000), 2nd ed., Inst. Geo. Surv. Ethiopia, Addis Ababa, Ethiopia.

Mogessie, A., Krenn, K., Schaflechner, J., Koch, U., Egger, T., Goritchnig, B., and Bauernfeind, D. (2002). A geological excursion to the Mesozoic sediments of the Abay Basin (Blue Nile), recent volcanic of the Ethiopian Main Rift, And basement rocks of the Adola Rea, Ethiopia. Mitt.Österr. Miner.Ges.147:43–74.

Pantelidis, L. (2009). Rock slope stability assessment through rock mass classification systems. Int. J. Rock Mech. and Min. Sci. 46:315–325.

Parise, M., and Jibson R. W. (2000). A seismic landslide susceptibility rating of geological units based on analysis of characteristics of landslides triggered by the 17 January 1994 Northridge, California Earthquake. Engineering Geology 58. Pp 251-270.

Poppe, L., Frankl, A., Poesen, J., Teshageradmasu, Dessie, M., Adgo, E. and Nyssen, J. (2013). geomorphology of the Lake Tana Basin, Ethiopia. J. Maps 9(3):431–437.

Price, D. G. (2009). Engineering geology principles and practice. Springer-Verlag, Berlin Heidelberg, Germany, 450 PP.

Raghuvanshi, T. K., Ibrahim, J.and Ayalew, D. (2014). Slope stability susceptibility evaluation parameter (SSEP) rating scheme – an approach for landslide hazard zonation. J. Afr. Earth Sci. 99:595–612.

Russo, A., Getaneh Assefa, and Balemwal Atinafu (1994). Sedimentary evolution of the Abay River (Blue Nile) basin, Ethiopia. N.Jb.Geol.Palaont. Mh. 291–308.

Seifu Kebede, Travi, Y., Tamiru Alemayehu, and Tenalem Ayenew (2005). Groundwater recharge, circulation, and geochemical evolution in the source region of the Blue Nile River, Ethiopia. App. Geoch. 20:1658–1676.

Soeters, R., and Van Westen, C.J. (1996). Slope instability recognition analysis and zonation.

In: Turner K.T. And Schuster, R.L., Eds., landslides: investigation and mitigation, special

report no. 247, transportation research board national research council, Washington Dc.,129-177

Suradi, M., And Fourie, A. (2014). The effect of rainfall patterns on the mechanisms of shallow slope failure. Aceh Int. J. Sci. Technology 3(1):1–18.

Tenalem Ayenew and Barbieri, G. (2005). Inventory of landslides and susceptibility mapping

In the Dessie area, Northern Ethiopia. Eng. Geol.77: 1-15.

Van Westen, C.J., Rengers, N., Soeters, R. (2003). Use of Geomorphological Information in

Indirect Landslide Susceptibility Assessment. In: Natural Hazards Vol. 30. Kluwer

Academic Publishers: 330-419.

Van Westen, C.J., (1993). Remote Sensing and Geographic Information Systems for

Geologic Hazard Mitigation. In: Space Congress, Bremen, Germany, Vol.

Environmental Assessment of Geological Hazards: 63-71.

Varnes, D. J. And the international association of engineering geology commission on landslide and other mass movements on slopes (1984). Landslide hazard zonation: a review of principles and practice (ISBN 92-3-101895-7) United Nations Educational, Scientific and Cultural Organization (UNESCO), 7 places de Fontenoy, 75700 Paris, France, 60 pp.

Wang, X., Niu, R. (2009). Spatial forecast of landslides in three gorges based on spatial data mining. Sensors 9, 2035–2061.

Wolela Ahmed (2009). Sedimentation and depositional environments of the Barremian-Cenomanian Debre Libanose Sandstone, Blue Nile (Abay) basin, Ethiopia. Cretaceous Research 30(5):1133–1145.

Wolela Ahmed. (2010). Diagenetic evolution of the Ansian – Pliensbachian Adigrat sandstone, Blue Nile Basin, Ethiopia. J. Afr. Earth Sci. 56(1):29–42.

Wolela Ahmed (2008). Sedimentation of The Triassic – Jurassic Adigrat sandstone formation, Blue Nile (Abay) Basin, Ethiopia. J.Afr. Earth Sci.52:30–42.

Zare, M., Jimenez, R., Khalokakaie, R., And Jalali, S. E. (2011). A probabilistic systems methodology to analyze the importance of factors affecting the stability of rock slopes. Eng. Geo. 118(3–4):82–92.

Zhao, L., Cao, J., Zhang, Y. and Luo, Q. (2015). Effect of hydraulic distribution on the stability of a plane slide rock slope under the nonlinear Barton-Bandis failure criterion. Geomech. and Eng. 8(3):391–414.

Tables

Table1: Data source used for landslide hazard mapping

Particulars	Map	GIS data type	Source
Landslide Inventory	Landslide Inventory Map	Polygon coverage	Google Earth Imagery, Historical record, and Field Survey
Geology and soil type	Lithology Map	Polygon coverage	Adopted from Tefera et al. (1996)
	Soil map	Polygon coverage	Extensive Field Survey
Digital Elevation Model (DEM)	Slope angle map	Grid	DEM 30m from USGS using ArcGIS 10.5 software
	Slope aspect map		
	Elevation map		
	Slope curvature map		
Hydrology	Distance to drainage	Grid	Developed from DEM and buffering using distance to Euclidian
Geological structure	Distance to fault	Grid	
Land use land cover	Land use land cover Map	Polygon coverage	Field Survey, Sentinel 2 images, and Google Earth

Table 2 Hazard index for various classes of causative factors.

Causative factors and corresponding factor class	landslide did not occur		landslide occurs		Hazard index (b/a)	Percent landslide
	Count	Ratio (a) (%)	Count	Ratio (b) (%)		
(a) Lithology						
Adigrat formation	150	0.08	8,418	10.49	127.26	86.06
Ashangi formation	429	0.23	1,443	1.8	7.67	5.19
Tarmaber formation	1,719	0.94	1,297	1.61	1.72	1.16
Alluvial soil	6,716	3.67	18,991	23.66	6.44	4.35
Colluvial soil	20,217	11.06	41,349	51.51	4.66	3.15
Residual soil	153,605	84.01	8,778	10.94	0.13	0.09
Total	182,836	100	80,276	100	147.87	100
(b) Slope(degree)						
0–5	22,197	12.14	1,310	1.63	0.13	1.61
5–14	13,450	7.36	9,110	11.35	1.54	18.44
14–25	17,956	9.82	17,981	22.40	2.28	27.27
25–35	69,471	38	16,859	21	0.55	6.61
35–45	44,192	24.17	13,393	16.68	0.69	8.25
>45	15,570	8.52	21,623	26.94	3.16	37.82
Total	182,836	100	80,276	100	8.36	100
(c) Aspect						
Flat	117	0.06	14	0.02	0.27	2.87
N	11,508	6.29	5,203	6.48	1.03	10.83
Ne	21,390	11.7	4,929	6.14	0.52	5.52
E	22,599	12.36	2,419	3.01	0.24	2.56
Se	23,520	12.86	2,887	3.6	0.28	2.94
S	21,956	12.01	5,207	6.49	0.54	5.68
Sw	23,173	12.67	11,026	13.74	1.08	11.4
W	23,719	12.97	19,313	24.06	1.85	19.51
Nw	24,457	13.38	21,716	27.05	2.02	21.27

Nnw	10,397	5.69	7,562	9.42	1.66	17.42
Total	182,836	100	80,276	100	9.51	100
(d) Elevation (m)						
1283-1544	1,078	0.59	14,998	18.68	31.68	65.29
1544-1764	5,302	2.9	16,944	21.11	7.28	15
1764-1994	7,394	4.04	14,266	17.77	4.39	9.06
1994-2221	8,781	4.8	19,112	23.81	4.96	10.22
2221-2500	160,280	87.66	14,956	18.63	0.21	0.44
Total	182,836	100	80,276	100	48.52	100
(e) Landuse/ landcover						
Forest	3,296	1.8	1,122.5	1.40	0.78	1.43
Urban	3,222	1.76	0	0	0	0
Grazing land	40,909	22.37	634.5	0.79	0.04	0.07
Bush land	11,113	6.08	18,159.8	22.62	3.72	6.86
Barren land	904	0.49	19,427.5	24.2	48.93	90.25
Cultivated land	123,391	67.49	40,931.8	50.99	0.76	1.39
Total	182,836	100	80,276	100	54.22	100
(F) Curvature						
Concave (+ve)	89,883	49.16	39,551	49.27	1	36.49
Flat (0)	2,705	1.48	877	1.09	0.74	26.89
Convex (-ve)	90,248	49.36	39,848	49.64	1.01	36.62
Total	182,836	100	80,276	100	2.75	100
(G) Distance from fault						
0-500	24,449	13.37	62,576.5	77.95	5.83	85.74
500-2000	42,633	23.32	16,070.5	20.02	0.86	12.63
2000-2500	38,107	20.84	765.5	0.95	0.05	0.67
2500-5000	36,219	19.81	67.5	0.08	0	0.06
5000-6500	31,689	17.33	773.5	0.96	0.06	0.82
> 6500	9,738	5.33	22.5	0.03	0.01	0.08

Total	182,836	100	80,276	100	6.8	100
(H) Distance from drainage						
0-298	58,468	31.98	36,003.4	44.85	1.4	28.6
298-604	52,082	28.49	20,484.4	25.52	0.9	18.27
604-902	39,240	21.46	12,524.4	15.6	0.73	14.82
902-1249	26,208	14.33	7,608.4	9.48	0.66	13.48
1249-2055	6,840	3.74	3,655.4	4.55	1.22	24.82
Total	182,836	100	80,276	100	4.9	100

Table 3 Weightings, hazard index, and hazard class for causative factors.

Causative factors (j)	Causative factor class (i)	Weighting (Wj)	Hazard index (Hji)	Hazard index scaled to 1 (Hji)	Hazard class
Lithology	Adigrat formation	1	127.26	1	5
	Ashangi formation		7.67	0.06	2
	Tarmaber formation		1.72	0.01	1
	Alluvial soil		6.44	0.05	1
	Colluvial soil		4.66	0.04	1
	Residual soil		0.13	0	1
Slope (degree)	0–5	1	0.13	0.04	1
	5–14		1.54	0.49	4
	14–25		2.28	0.72	4
	25–35		0.55	0.17	3
	35–45		0.69	0.22	4
	>45		3.16	1	5
Aspect	Flat	1	0.27	0.13	3
	N		1.03	0.51	4
	NE		0.52	0.26	4
	E		0.24	0.12	2
	SE		0.28	0.14	3
	S		0.54	0.27	4
	SW		1.08	0.54	4
	W		1.85	0.92	5
	NW		2.02	1	5
	NNW		1.66	0.82	5
Elevation (m)	1283-1544	1	31.68	1	5
	1544-1764		7.28	0.23	4
	1764-1994		4.39	0.14	3
	1994-2221		4.96	0.16	3

	2221-2500		0.21	0.01	1
Landuse/ landcover	forest	1	0.78	0.02	1
	urban		0	0	1
	grazing land		0.04	0	1
	bushland		3.72	0.08	2
	barren land		48.93	1	5
	cultivated land		0.76	0.02	1
Curvature	concave (+ve)	1	1	0.99	5
	flat (0)		0.74	0.73	4
	convex (-ve)		1.01	1	5
Distance from fault	0-500	1	5.83	1	5
	500-2000		0.86	0.15	3
	2000-2500		0.05	0.01	1
	2500-5000		0	0	1
	5000-6500		0.06	0.01	1
	> 6500		0.01	0	1
Distance from drainage	0-298	1	1.40	1.00	5
	298-604		0.90	0.64	4
	604-902		0.73	0.52	4
	902-1249		0.66	0.47	4
	1249-2055		1.22	0.87	5

Table 4 Hazard index classification.

Hazard class	Hazard index (Hji) classification	Hazard class name
1	0.0–0.05	No hazard (NH)
2	0.05–0.12	Low hazard (LH)
3	0.12–0.18	Medium hazard (MH)
4	0.18–0.75	High hazard (HH)
5	0.75–1.0	Very high hazard (VHH)

Figures

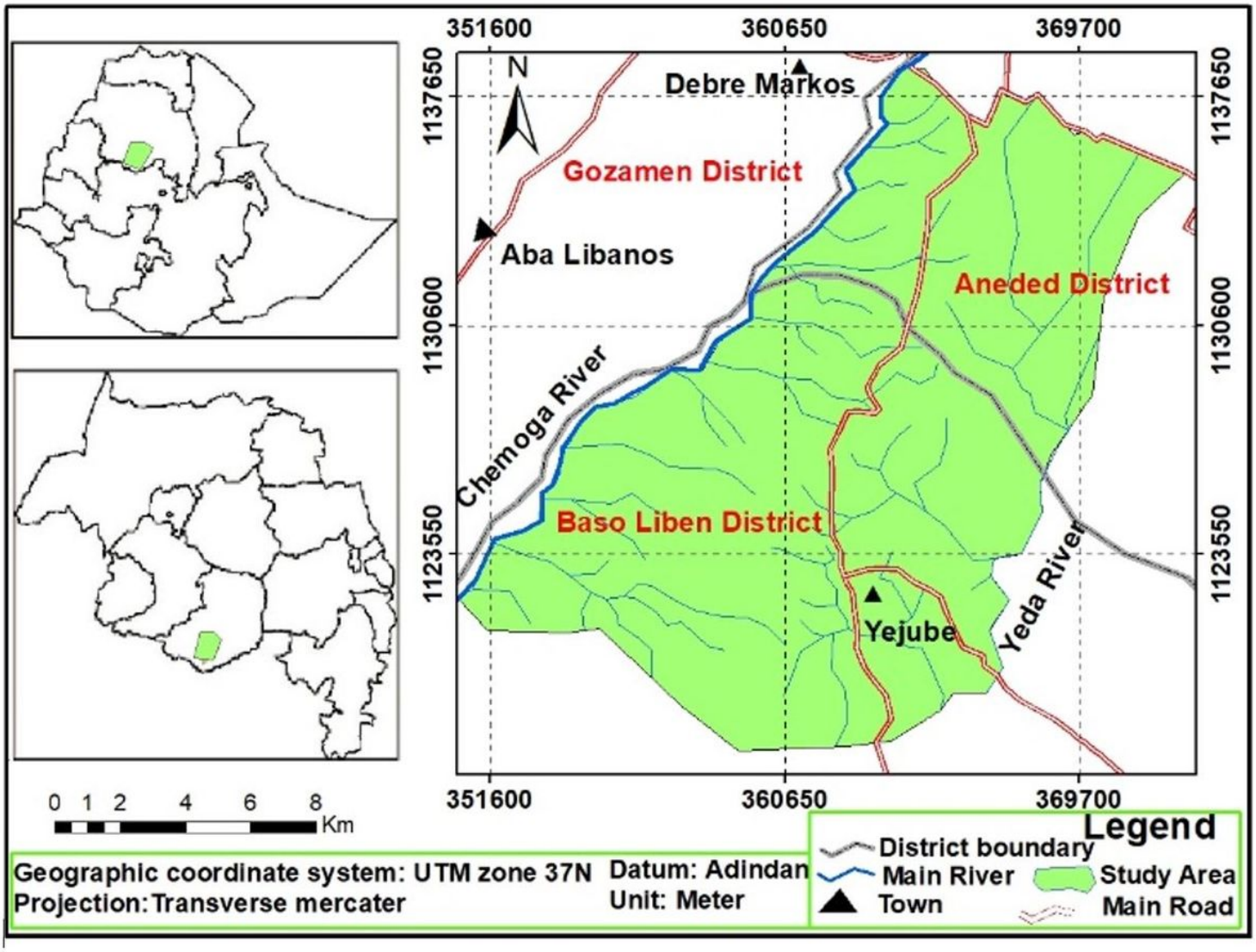

Figure 1

Study area. Note: The designations employed and the presentation of the material on this map do not imply the expression of any opinion whatsoever on the part of Research Square concerning the legal

status of any country, territory, city or area or of its authorities, or concerning the delimitation of its frontiers or boundaries. This map has been provided by the authors.

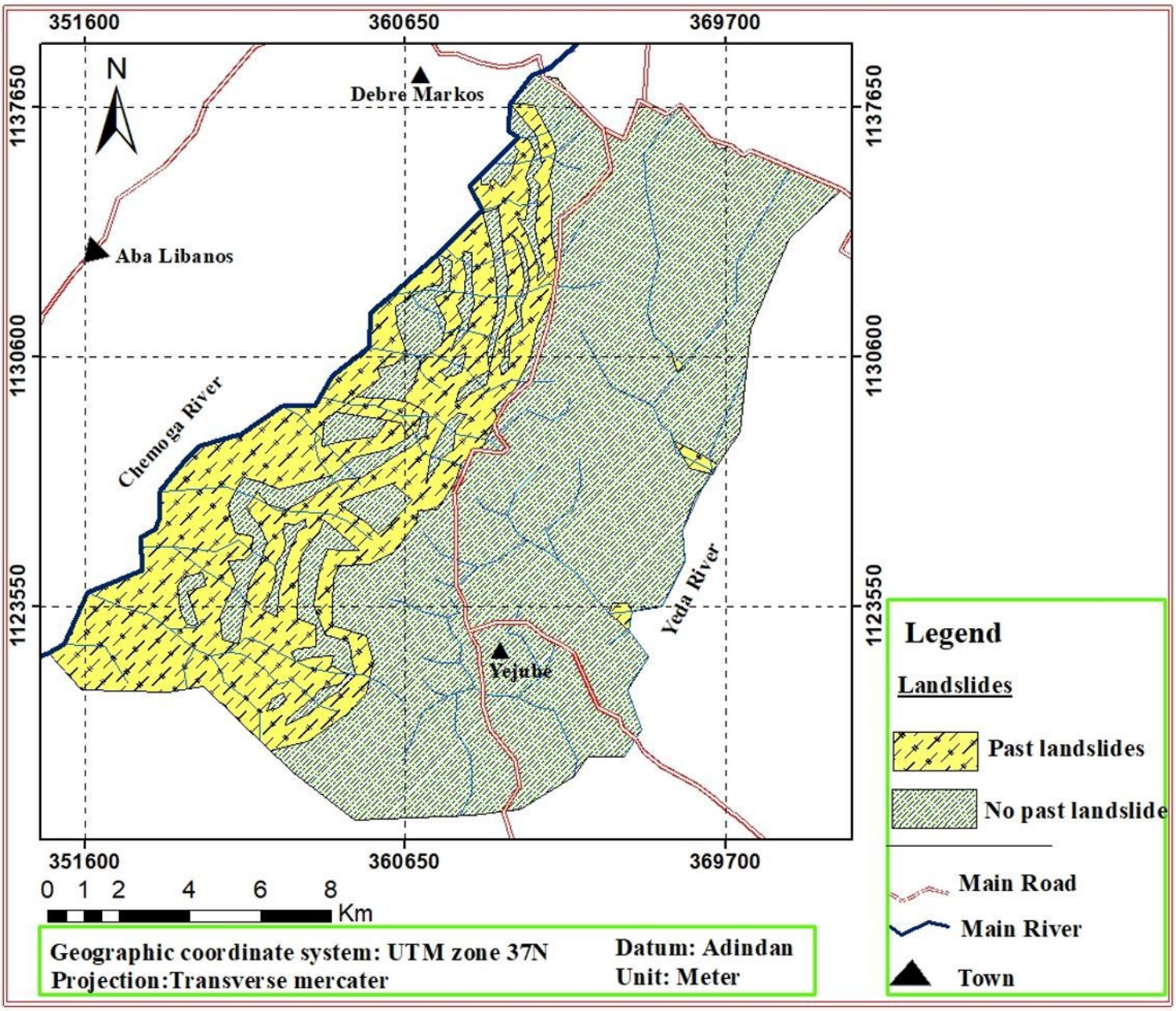

Figure 2

Inventory Mapping. Note: The designations employed and the presentation of the material on this map do not imply the expression of any opinion whatsoever on the part of Research Square concerning the legal status of any country, territory, city or area or of its authorities, or concerning the delimitation of its frontiers or boundaries. This map has been provided by the authors.

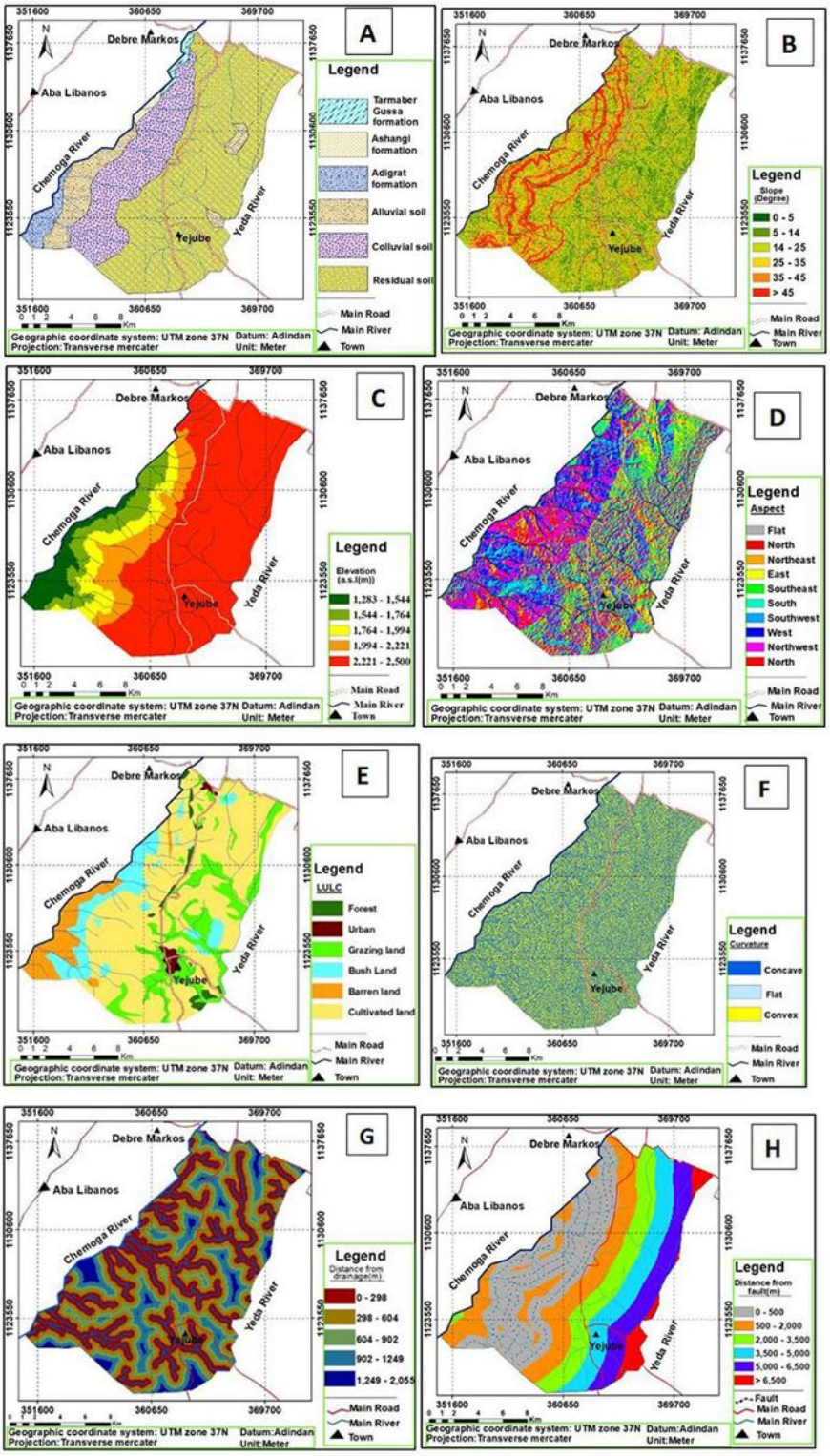

Figure 3

Lithology and Soil Mass(A), Slope(B), Elevation(C), Aspect(D), LULC(E), Curvature(F), Distance to Drainage(G), Distance to Fault(H). Note: The designations employed and the presentation of the material on this map do not imply the expression of any opinion whatsoever on the part of Research Square concerning the legal status of any country, territory, city or area or of its authorities, or concerning the delimitation of its frontiers or boundaries. This map has been provided by the authors.

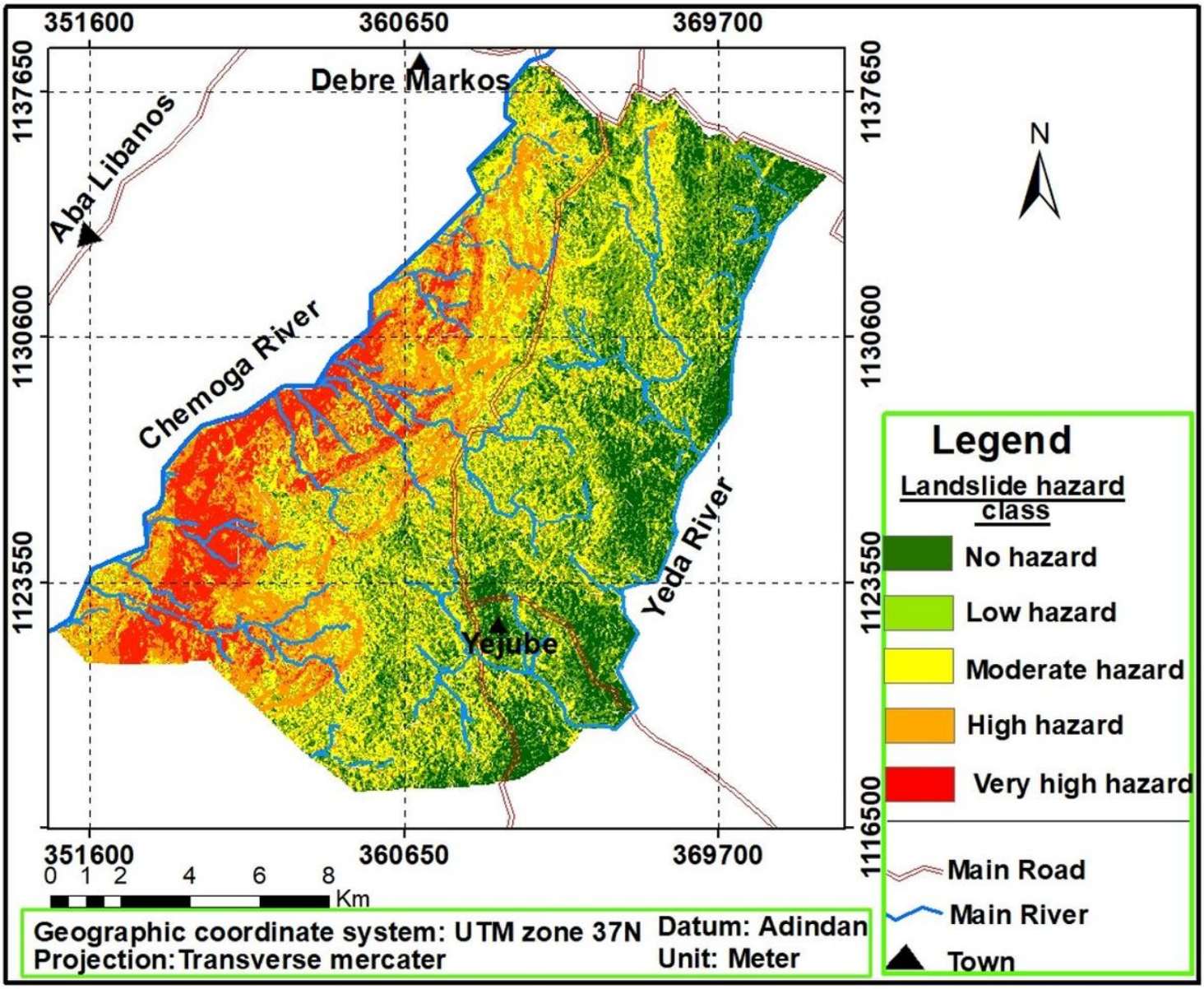

Figure 4

Landslide hazard zonation map. Note: The designations employed and the presentation of the material on this map do not imply the expression of any opinion whatsoever on the part of Research Square concerning the legal status of any country, territory, city or area or of its authorities, or concerning the delimitation of its frontiers or boundaries. This map has been provided by the authors.

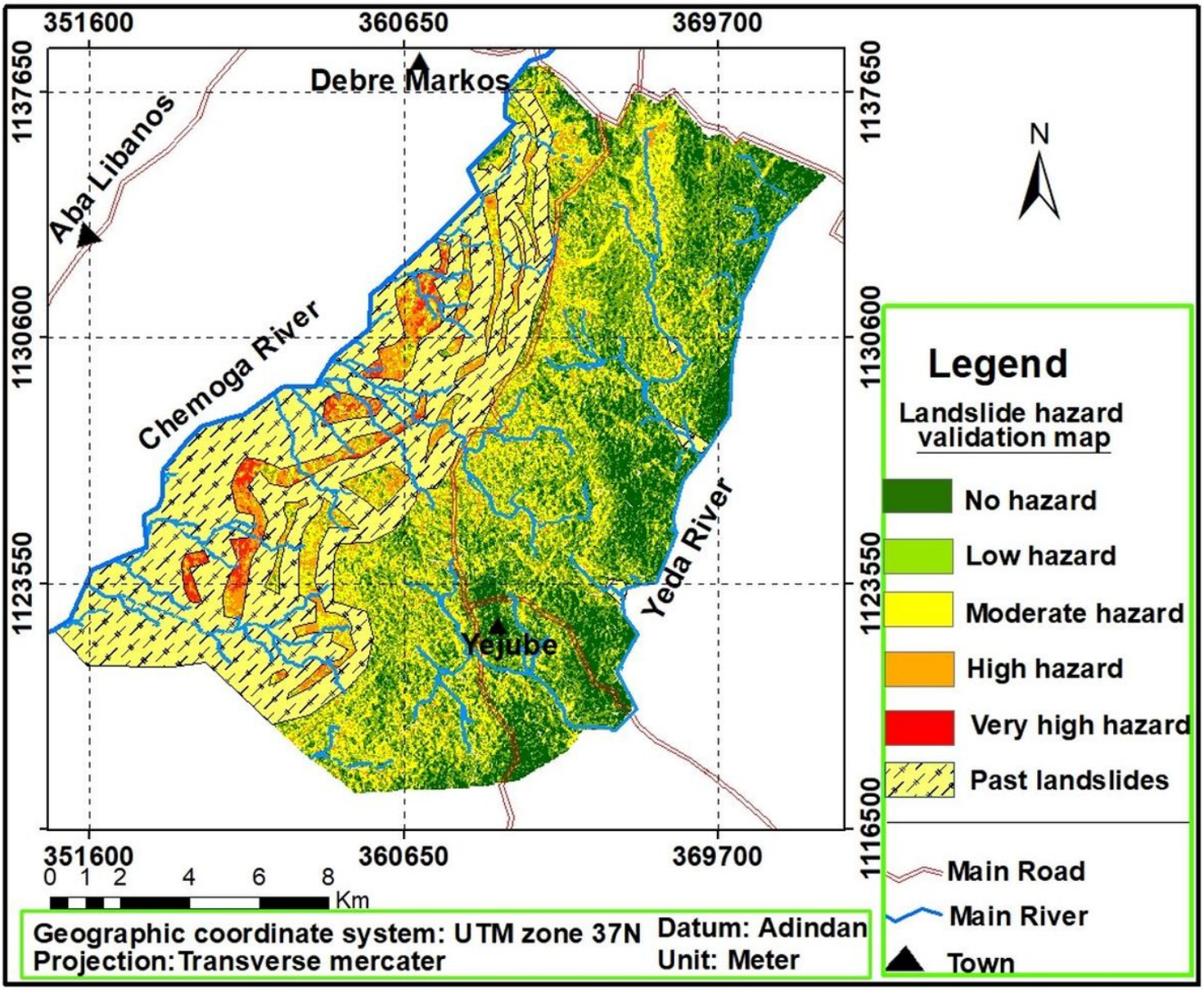

Figure 5

Validation of LHZ ma. Note: The designations employed and the presentation of the material on this map do not imply the expression of any opinion whatsoever on the part of Research Square concerning the legal status of any country, territory, city or area or of its authorities, or concerning the delimitation of its frontiers or boundaries. This map has been provided by the authors.